NAT'L INST. OF STAND & TECH
A11106 964799
NIST
PUBLICATIONS
REFERENCE

NISTIR 7373

Chemical and Physical Characterization of Poly(p-phenylene-2,6-benzobisoxazole) Fibers Used in Body Armor: Temperature and Humidity Aging

QC
100
.U56
#7373
2006

NIST
National Institute of Standards and Technology
Technology Administration, U.S. Department of Commerce

NISTIR 7373

Chemical and Physical Characterization of Poly(p-phenylene-2,6-benzobisoxazole) Fibers Used in Body Armor: Temperature and Humidity Aging

Joannie Chin, Eric Byrd, Cyril Clerici, Mounira Oudina and Lipiin Sung
Polymeric Materials Group
Materials and Construction Research Division
Building and Fire Research Laboratory

Amanda Forster and Kirk Rice
Office of Law Enforcement Standards
Electronics and Electrical Engineering Laboratory

Sponsored by:
National Institute of Justice
Office of Justice Programs

U.S. DEPARTMENT OF COMMERCE
Carlos M. Gutierrez, Secretary
TECHNOLOGY ADMINISTRATION
Robert C. Cresanti, Under Secretary of Commerce for Technology
NATIONAL INSTITUTE OF STANDARDS AND TECHNOLOGY
William Jeffrey, Director

ABSTRACT

In recent years, poly(p-phenylene-2,6-benzobisoxazole) (PBO) fibers have become prominent in high strength applications such as body armor, ropes and cables, and recreational equipment. The objectives of this study were to expose woven PBO body armor panels to elevated temperature and moisture, and to analyze the chemical, morphological and mechanical changes in PBO yarns extracted from the panels. A 30 % decrease in yarn tensile strength, which was correlated to changes in the infrared peak absorbance of key functional groups in the PBO structure, was observed during the 26 week elevated temperature/elevated moisture aging period. Substantial changes in chemical structure were observed via infrared spectroscopy, as well as changes in polymer morphology using microscopy and neutron scattering. When the panels were removed to an ultra-dry environment for storage for 47 weeks, no further decreases in tensile strength degradation were observed. In a follow-on study, fibers were sealed in argon-filled glass tubes and exposed to elevated temperature; less than a 4 % decrease in tensile strength was observed after 30 weeks.

Key Words: body armor, poly(p-phenylene-2,6-benzobisoxazole) (PBO), attenuated total reflectance (ATR), infrared (IR) spectroscopy, fiber, yarn, moisture sorption, tensile strength, hydrolysis, laser scanning confocal microscopy, atomic force microscopy, small angle neutron scattering

Introduction and Objectives

In recent years, high performance fibers based on poly(p-phenylene-2,6-benzobisoxazole) (PBO) have become prominent in high strength applications such as body armor, ropes and cables, and recreational equipment. Problems with the performance and durability of PBO-based body armor became apparent to the law enforcement community in the summer of 2003, when ballistic penetration of PBO-based body armor occurred in two separate incidents.

The first incident involved the shooting of a police officer near Pittsburgh, PA (hereinafter referred to as the "officer") in June 2003. The bullet pierced the officer's PBO-based body armor, which had been manufactured less than 8 months earlier. Mechanical testing of the yarns taken from the officer's vest indicated a 30 % decrease in tensile strength relative to yarns taken from new, unworn PBO-based vests of the same model. Subsequently, another incident involving the ballistic penetration of PBO-based body armor occurred that same year, but the evidentiary circumstances surrounding these incidents are more complicated and, as such, are not be discussed here.

These events prompted the Department of Justice (DOJ) and then-U.S. Attorney General John Ashcroft to announce a Body Armor Safety Initiative on November 18, 2003 [1], which tasked the National Institute of Justice (NIJ), the research, development, and evaluation arm of DOJ, to address technical issues associated with PBO-based body armor. In response to this initiative, NIST's Office of Law Enforcement Standards (OLES) and research groups within the NIST laboratories undertook a parallel, multi-phase effort to characterize chemical and physical degradation of PBO fiber and to correlate the observed degradation to body armor durability.

In previous work performed at NIST, a comparative analysis study was carried on the officer's vest and new, unused vests of the same make and model. The primary findings in this work were that yarns from the officer's vest had tensile strengths approximately 30 % lower than yarns from new vests of the same make and model, and that a breakdown in the molecular structure of the PBO chains was revealed by infrared analysis of the vest yarns [2].

Data from the manufacturer and the published literature have revealed the moisture vulnerability of PBO fibers [3,4]. In an attempt to quantify this vulnerability, and to determine if correlations existed between moisture exposure, tensile strength degradation and ballistic failure, an experimental study was designed in which newly-manufactured body armor constructed from PBO were exposed to elevated temperature and relative humidity in an environmental chamber. When yarn tensile strengths had decreased by 30 % relative to the initial tensile strength, the exposure was terminated and ballistic testing was carried out on the exposed vest panels. The ballistic testing of the aged vests will be documented in a separate report.

The primary goals of the work described in this report were to:

- Monitor tensile strength degradation in PBO yarns extracted from body armor exposed to elevated temperature and relative humidity as a function of exposure time.
- Monitor chemical and physical changes in PBO yarns extracted from body armor exposed to elevated temperature and relative humidity as a function of exposure time.
- Determine if any correlations exist between chemical hydrolysis and tensile strength degradation in PBO yarns

Future phases of this research program will address degradation mechanisms, accelerated aging and prediction of ballistic fiber service life.

Experimental Procedures*

Materials—Commercial, non-deployed body armor manufactured for this study consisted of a ballistic panel constructed from 20 layers of woven PBO fabric stacked and diagonally stitched together, inserted in a water vapor-permeable fabric liner, and placed in a cotton fabric carrier. For testing and analyses, PBO yarns were extracted from the exposed vest panels at predetermined inspection times.

Environmental Exposure— 24 ballistic panels enclosed in liners and carriers (shown in Figure 1) were aged in a Cincinnati Sub-Zero Z32 environmental chamber at 50 °C and 60 % relative humidity (RH) for 84 d, and then 60 °C and 37 % RH for an additional 73 d. The increase in temperature to 60 °C and decrease in relative humidity to 37 % were intended to accelerate the kinetics of fiber degradation by increasing the temperature while maintaining the same absolute water content in the environment. Following the completion of the environmental chamber aging, 18 panels were removed for ballistic testing, while the remainder was stored in the chamber at 25 °C and 5 % RH for an additional 332 d.

To more accurately monitor temperature and relative humidity in the large chamber area, a number of temperature and RH sensors were distributed throughout the interior of the chamber as well as in the interior of the vest panels. These temperature

* Certain commercial equipment, instruments or materials are identified in this paper in order to specify the experimental procedure adequately. Such identification is not intended to imply recommendation or endorsement by the National Institute of Standards and Technology, nor is it intended to imply that the materials or equipment identified are necessarily the best available for this purpose.

and RH sensor data were logged and stored via a data acquisition system and a desktop computer.

Yarn Extraction Procedure— At each inspection time, 15 horizontally oriented yarns were extracted from layers 1, 5, 15, 19 in two different ballistic panels (labeled 089 and 055, respectively), with two layers of each panel sampled every 2 weeks. Seams were cut from the bottom 5 cm to 6 cm of the ballistic panel to free the layers. As shown in Figure 2, individual yarns were loosened and extracted one by one from the lower half of the layer using a small hook, and taped down on cleaned aluminum foil-wrapped cardboard holders. Each yarn was labeled with panel number, layer number and yarn number. Nitrile gloves were worn throughout the entire procedure to prevent contamination of the yarns. From the 15 yarns extracted, three were reserved for Fourier transform infrared (FTIR) spectroscopy analysis, while the remaining yarns were used for tensile testing.

Moisture Sorption Analysis—Moisture absorbed by the yarn specimens during the temperature/humidity exposure period was measured using a Hiden IGAsorp Moisture Sorption Analyzer. The IGAsorp software monitors the temporal changes in the mass of a specimen subjected to prescribed temperature and relative humidity conditions, and calculates equilibrium parameters via curve fitting. Specimens for sorption analysis were prepared by disassembling between 5 mg to 7 mg of yarn into individual filaments to prevent capillarity effects from dominating the sorption process. Prior to beginning a sorption experiment, specimens were dried in the moisture sorption analyzer at ≈ 0 % RH and the prescribed temperature at which the sorption experiment would be carried out. Moisture uptake was measured at 50 ^{o}C and 60 % RH as well as at 60 ^{o}C and 37 % RH.

The water sorption isotherm was generated using the isothermal mapper mode at 40 °C within a range of 0 % RH to 95 % RH. Results are the average of two specimens. The standard uncertainty of these measurements is typically 0.02 mass %.

Tensile Testing of Yarns and Fibers—Tensile testing of yarns was carried out in accordance with ASTM D2256-02, "Standard Test Method for Tensile Properties of Yarn by the Single-Strand Method", using an Instron Model 4482 screw-driven universal test frame equipped with a 91 kg load cell, and pneumatic yarn and chord grips (Instron model 2714-006). Strain measurements were taken with an Instron non-contacting Type 3 video extensometer in conjunction with black foam markers placed approximately 2.5 cm apart in the gage section of the yarn. Grip separation was 7.9 cm and cross-head speed was 2.3 cm/min. In this study, yarns were nominally 38.1 cm long, and given 60 twists on a custom-designed yarn twisting device. The standard uncertainty of measured tensile strengths, percent strain to break, modulus, and break energy are typically ± 3 %, ± 3 %, ± 3 %, and ± 4 %, respectively.

Tensile tests were also carried out on individual single fibers utilizing a TA Instruments RSA III, a dynamic mechanical thermal analyzer (DMTA) equipped with transient testing capability. Specimen gage length was 25 mm and specimen extension rate was 0.001 mm/s. A minimum of ten fibers were analyzed from one extracted yarn per sampling interval. Standard uncertainty of tensile strengths measured using this method is typically ± 9 %.

Fourier Transform Infrared (FTIR) Spectroscopy—Infrared analysis was carried out using a Nicolet Nexus FTIR equipped with a mercury-cadmium-telluride (MCT) detector and a SensIR Durascope attenuated total reflectance (ATR) accessory. Dry air

was used as the purge gas. Consistent pressure on the yarns was applied using the force monitor on the Durascope. FTIR spectra were recorded at a resolution of 4 cm^{-1} between 4000 cm^{-1} and 700 cm^{-1} and averaged over 128 scans. Three different locations on each yarn were analyzed. Spectral analysis, including spectral subtraction, was carried out using a custom software program developed in the Polymeric Materials Group at NIST [5]. All spectra were baseline corrected and normalized using the aromatic C-H deformation peak at 848 cm^{-1}. Standard uncertainties associated with this measurement are typically $\pm$ 1 cm^{-1} in wavenumber and $\pm$ 1% in peak intensity.

Small Angle Neutron Scattering—Small angle neutron scattering (SANS) measurements were performed at the NIST Center for Neutron Research using the 30 m SANS instrument. Samples of virgin spool yarn, unaged vest yarn, and vest yarn aged for 157 d in the environmental exposure study were soaked in 99 % pure deuterated water (D_2O) in a glass vial for one week, and then transferred to a flat cell with diameter of 2.54 mm and path length of 1 mm immediately before the measurement. Within the cell, yarns were positioned in a random orientation. SANS measurements were conducted at 5 h and 36 h following D_2O immersion to monitor changes in the scattering profiles, which will reflect the exchange of D_2O and H_2O in the pore spaces of the fiber.

After calibration and taking into account the sample transmission and thickness, two-dimensional SANS images, shown in Figure 3(a), were averaged azimuthally to produce a one-dimensional plot of the absolute scattered intensity as a function of the scattering wave vector q ($q= 4\pi \sin(\theta/2)/\lambda$, where θ is the scattering angle and λ is the wavelength). This plot is also referred to as the *scattering profile.* If the two-dimensional scattering image exhibits a preferred orientation, a sector average was

accounted for over an azimuth angle of 15 degrees, as indicated in Figure 3(b). A peak in the scattering profile or a ring in the scattering image at scattering wave vector q indicates the existence of an ordered micro/nanodomains with a characteristic average length $d = 2\pi/q$ [6].

Atomic Force Microscopy—The nanoscale surface morphology of the fibers was observed using atomic force microscopy (AFM), using a Dimension 3100 scanning probe microscope (Veeco Metrology) in tapping mode. All scans were taken using commercial silicon microcantilever probes (Veeco Metrology) with a manufacturer-reported radius of < 10 nm. Topographic and phase images were obtained simultaneously using a resonance frequency of approximately 300 kHz for the probe oscillation and a free-oscillation amplitude of 62 nm ± 2 nm. Between 6 and 10 micrographs were obtained for each sample, with representative images reported here.

Laser Scanning Confocal Microscopy—A Zeiss Model LSM510 reflection laser scanning confocal microscope (LSCM) was used to characterize the surface morphology of the fibers. The incident laser wavelength was 543 nm. By moving the focal plane in the z-direction, a series of single images (optical slices) can be stacked and digitally summed over the z-direction to obtain a 3-D image. All images presented here are 2-D projections of a stack of 3-D images. The *z*-direction step size was 0.1 μm using a 150x objective.

Sealed Tube Study—Approximately 200 specimens having a length of 51 cm were cut from a spool of virgin PBO yarn supplied by the manufacturer. Each length of yarn was inserted into a 6 mm diameter glass tube, which was then evacuated and back-filled with argon, after which the tube ends were heat-fused. Tubes were then placed in a

55 °C circulating air oven and removed at periodic intervals for tensile testing and FTIR analysis. A thermocouple sealed into one of the argon-purged tubes confirmed that the temperature in the tube reached 55 °C after being placed in the oven. Between 10 and 13 specimens were randomly selected and tested at predetermined time intervals. Elapsed time between removal of the yarn from the glass tube and either tensile testing or infrared analysis was less than 5 min.

Results and Discussion

PBO is a member of the benzazole polymer family and is characterized by the heterocyclic benzobisoxazole group in its main chain structure. The chemical structure of the PBO repeat unit is shown in Figure 4. The conjugated benzobisoxazole and phenyl rings in the PBO repeat unit contribute to extended π-electron delocalization and molecular rigidity, which provides high thermal stability and outstanding mechanical properties. PBO fibers, as are the majority of the polybenzazole-based fibers, are extremely strong, tough and stiff, with tensile strengths and moduli greater than that of polyaramid or ultra-high molecular weight polyethylene. The chemistry and processing of PBO and related polymers have been documented elsewhere [7,8] and are not discussed further.

Figure 5 shows the relative humidity sensor readings from the interior of the environmental chamber as well as from the interior of the ballistic panel, during a period when the relative humidity setting within the chamber was deliberately decreased and then increased. The sensor inside the ballistic panel responded to these changes rapidly,

indicating that water vapor in the external environment is readily transmitted through both the cotton carrier and the moisture-permeable liner into the ballistic panel. For this particular model of body armor, moisture that is present in the external environment or on the wearer's body is readily transported into the ballistic fabric.

Moisture sorption measurements were carried out on virgin PBO spool yarn to determine the mass uptake of water during the temperature/humidity exposure period. In the desorption stage of the experiment, the moisture content of the virgin PBO yarn stored under ambient conditions was approximately 0.8 mass % to 0.9 mass %, which compares well with mass loss at 110 °C measured via thermogravimetric analysis (TGA). As shown in Figure 6, the equilibrium moisture content of the virgin yarn at 50 °C and 60 % RH and 60 °C and 37 % RH is (1.56 ± 0.02) mass % and (0.81 ± 0.02) mass %, respectively, with the higher temperature condition resulting in a lower mass uptake of water. Lower moisture uptake at higher temperatures has also previously been observed for poly(p-phenylene terephthalamide) (PPTA), another commonly used ballistic material [9, 10], and nylon 6,6 [11].

Figure 6 also shows the sorption behavior of the PBO yarn at 50 °C and 60 % RH followed by an in-situ change in the experimental conditions to 60 °C and 37 % RH. The moisture content of the yarn decreases at the higher temperature, which is consistent with previous observations, but does not completely reach the moisture content of the yarn initially equilibrated at 60 °C and 37 % RH. One possible explanation for this difference of 0.2 mass % between the two equilibrium moisture levels is that the microvoids in the fiber trap adsorbed water, and this trapped water is not easily removed at the temperature and relative humidity level used [12].

Figure 7 shows the moisture sorption isotherm for virgin spool yarn at 40 °C, which is approximately the temperature of the human body under normal conditions. The sorption isotherm provides information on the water sorption in PBO fibers as a function of relative humidity at a given temperature. At high levels of relative humidity, the moisture content of the PBO fibers approaches 7 mass % at 95 % RH. Analysis of the sorption isotherm was carried out using the Guggenheim-Anderson-de Boer (GAB) model, which has been shown suitable for describing water sorption isotherms of a variety of polymers over a wide RH range [13]. The experimental water sorption isotherm was fitted by the GAB equation, which has the form:

$$m_{a_w} = \frac{m_{GAB} C_{P,GAB} k a_w}{(1 - k a_w)} \times \frac{1}{1 + (C_{P,GAB} - 1) k a_w} \tag{1}$$

where a_w is the water activity (i.e. RH/100), m_{aw} is the water content at a specific value of a_w' $C_{p,GAB}$ is the Guggenheim constant, m_{GAB} is the monolayer water content and k is a correction factor which is typically less than 1. To determine these parameters, the GAB equation is linearized to the following expression:

$$f_{GAB} = \frac{a_w}{(1 - k a_w) m_{a_w}} = \frac{1}{C_{p,GAB} m_{GAB} k} + \frac{C_{p,GAB} - 1}{C_{p,GAB} m_{GAB}} a_w \tag{2}$$

A plot of f_{GAB} versus a_w within the range $0.1 < a_w < 0.8$ gives a linear plot if a correct value of k is used, and whose intercept and slope are $\frac{1}{C_{p,GAB} m_{GAB} k}$ and $\frac{C_{p,GAB} - 1}{C_{p,GAB} m_{GAB}}$ respectively. The GAB parameters obtained for the sorption isotherm at 40 °C for the virgin yarn are shown in Figure 7. The residual sum of squares (RSS) values defined by

$RSS = \sum\left(m_{\text{exp}} - m_{\text{calc}}\right)$ show a good fit between the experimental data and the model over the entire range of relative humidity.

As shown in Figure 7, the moisture sorption isotherm of the PBO fibers at 40 °C displays an upward curvature which became more pronounced at higher relative humidity. The positive deviation from linearity, i.e. from Henry's law, at high relative humidity suggests that the clustering of water occurs in the fibers. The number of water molecules in a cluster can be estimated from the GAB parameters and φ, the volume fraction calculated as the ratio of the volume of sorbed water at the sorption equilibrium to the volume of dry polymer. Values of φ were determined from the moisture content using a fiber density of 1.54 g/cm^3 [3]. The cluster number, N_c, represents the average of excess water molecules in the vicinity of a given water molecule including itself, and can be expressed as follows [14]:

$$N_C = -(1-\varphi)\times\left[\frac{\varphi}{m_{GAB}C_{P,GAB}}\left(-2C_{P,GAB}ka_w + 2ka_w + C_{P,GAB} - 2\right) - 1\right] \qquad (3)$$

If N_c is equal to unity, then no clustering exists.

Figure 8 shows the number of water molecules per cluster in the PBO yarn as a function of relative humidity at 40 °C. In the relative humidity range from 0 % to 20 %, no clustering was observed. The number of water molecules increases in a near-linear fashion in the relative humidity range between 20 % and 60 %, coinciding with the point of inflection in the water sorption isotherm. In the range between 20 % and 60 %, N_c is approximately 2. Beyond 60 % RH, N_c increases rapidly up to 8.3 water molecules per clusters at 95 % RH. Cluster growth results when a higher affinity exists between water molecules than between water molecules and the fiber, and is also attributed to the

presence of microcavities and micro-cracks, which increase the capacity for moisture sorption.

The moisture sorption mechanism of PPTA, another commonly-used ballistic fiber, has been studied extensively by other researchers [9, 12]; however, little or no data on the moisture sorption behavior of PBO has been published until now. The chemical composition and the microstructure of fiber materials are two parameters that strongly influence water vapor sorption behavior. Kitagawa et al. proposed that the PBO fiber is composed of microfibrils and that capillary-like microvoids are present between the microfibrils [15]; a similar microstructure has also been attributed to PPTA [16,17,18]. In contrast to PPTA which contains amide and amino functional groups that are capable of hydrogen-bonding with water, PBO has functional groups that are polar in nature but not capable of hydrogen-bonding.

Table 1 shows tensile strengths of vest yarns subjected to environmental chamber aging as a function of exposure time. The tensile strength of unaged vest yarns is 4.8 GPa, compared to the virgin PBO spool yarn tensile strength of 5.3 GPa measured in our lab and 5.8 GPA reported by the manufacturer [3]. The difference between the tensile strengths of the unaged vest yarn and the virgin yarn is attributed to mechanical damage incurred in the weaving process.

At 50 °C and 60 % RH, average yarn tensile strength dropped from 4.8 GPa to 3.64 GPa after 84 d. The rate of tensile strength loss was determined not to be statistically different for yarns extracted from the two vests and appears to be near-linear with time. In an attempt to accelerate the rate of degradation, the chamber temperature was increased to 60 °C while maintaining the chamber moisture content at the same level

by decreasing the relative humidity to 37 %. Exposure continued for another 73 d, during which the average yarn tensile strength dropped from 3.64 GPa to 3.08 GPa. No additional decreases in tensile strength were observed during storage at 25 °C and 5 % RH. Average strain to failure during the exposure period dropped from 3.31 % to 2.17 % while the tensile modulus remained constant at around 145 GPa.

Tensile strengths of single fibers measured via DMTA are compared with yarn tensile strength data in Figure 9. In general, the fiber data track closely with and come close to overlapping the yarn data, when the data standard deviations are taken into account (which are greater for the single fiber than they are for the yarn). The advantage of testing single fibers as opposed to yarns is the amount of material needed for the respective tests: DMTA can be used to test fibers as short as 12 mm, whereas a full 51 cm is needed for a yarn tensile test on a typical universal test frame.

The interaction between materials and the infrared region of the electromagnetic spectrum provides valuable information on the molecular structure of organic materials, including organic polymers. Specific functional groups absorb at given frequencies corresponding to their vibrational modes. Changes in the intensities or frequencies of observed spectral peaks can be used to elucidate changes in the molecular structure of the compound. This type of information is valuable for mechanistic and kinetic studies of polymer degradation. The primary infrared bands in PBO are listed and assigned in Table 2. Peak identification and assignments are made on the basis of literature data [19, 20, 21, 22, 23] and studies carried out in our lab on benzoxazole and 2-phenyl benzoxazole model compounds.

ATR-FTIR analysis of extracted vest yarns was carried out concurrently with tensile testing. Figure 10 shows the ATR infrared spectra of the yarns prior to and after environmental aging for 157 d. Visual examination of the two spectra, which have been baseline-corrected and normalized, shows distinct peak intensity differences.

These differences are most easily analyzed using spectral subtraction, in which a reference spectrum is subtracted from the spectrum of a material of interest. This technique is often helpful in extracting specific chemical changes and providing information on the formation and depletion of specific functional groups. Figure 11 shows the difference spectra that result when the infrared spectrum of the non-exposed vest yarn is subtracted from each of the exposed vest yarn spectra. Downward-pointing, or negative, peaks in the difference spectra are attributed to species that are lower in concentration relative to the reference spectrum (the non-exposed vest yarn) and upward-pointing, or positive, peaks are either species that are higher in concentration relative to the reference material or are new species that were not originally present in the reference material.

Negative peaks observed at 914 cm^{-1}, 1056 cm^{-1}, and 1362 cm^{-1} are assigned to the vibrations associated with the benzoxazole ring [19], and grow progressively larger (more negative) with time. A positive peak at 1650 cm^{-1} in the region associated with amide carbonyl or carboxylic acid [24] also grew progressively larger with time. This observation suggests that benzoxazole ring-opening has occurred with the subsequent formation of benzamidophenol groups as depicted in Figure 12. Further breakdown of benzamidophenol groups could lead to the formation of aminophenol and benzoic acid groups, and the breadth of the peak at 1650 cm^{-1} allows for the possibility of benzoic acid

peak at 1680 cm^{-1} [24]. The growth of new peaks centered at 3300 cm^{-1} also points to the presence of amide N-H stretch or carboxylic acid O-H stretch.

Kim et al. [25] observed carboxylic acid peaks in the FTIR spectra of PBO that have undergone acid-catalyzed hydrolysis, with a concurrent decrease in the molecular weight evidenced by significant decrease in intrinsic viscosity, which is consistent with the chain scission mechanism. Evidence for PBO hydrolysis leading to carboxylic acid formation is also reported by So et al., who detected a peak at 1690 cm^{-1} attributed to carboxylic acid in the infrared spectrum of PBO, following exposure to severe hydrolytic conditions [26].

Support for the hydrolysis of benzoxazole to benzamide in low molecular weight compounds was given by Jackson et al [27]. When 2-phenylbenzoxazole (1) is heated in an acidic medium, N-(2-phenylhydroxybenzamide) (2) is first formed:

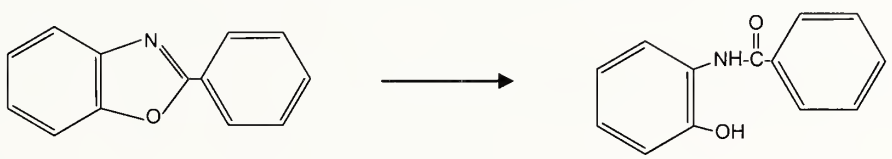

(1) (2)

N-(2-phenylhydroxybenzamide) can then further hydrolyze to 2-aminophenol and benzoic acid ((3) and (4), respectively), or re-convert to 2-phenylbenzoxazole (1):

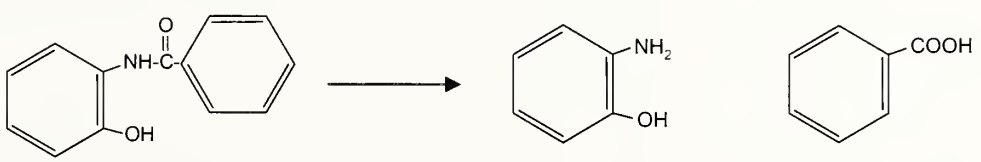

(2) (3) (4)

Two small peaks are observed at 1726 cm^{-1} and 1691 cm^{-1} in all yarns analyzed, and are shown on an expanded scale in Figure 13. These peaks have not been reported in any previous publications on PBO and have not been observed in our analysis of benzoxazole-containing model compounds. However, FTIR analysis of phenyl benzoate compounds revealed a match to these 2 peaks. 2-phenyl benzoate is an intermediate compound in the synthesis of PBO, which undergoes acyl migration to form the corresponding 2-phenylhydroxybenzamide, which then subsequently rearranges to form the benzoxazole ring structure [28]. It is possible that the phenyl benzoate peaks detected in the FTIR spectrum of PBO are due to residual intermediate products from the synthesis process. The presence of these residues is potentially detrimental to PBO properties, because benzoate linkages are not as chemically, hydrolytically, or thermally resistant as benzoxazole linkages, and each benzoate linkage exists at the expense of the more desirable benzoxazole functionality.

Figure 14 shows yarn tensile strength plotted against the absorbance of the negative peaks corresponding to the benzoxazole group. A positive correlation was observed between tensile strength and spectral absorbance of these peaks; that is, as the benzoxazaole group decreases in concentration due to hydrolysis, the tensile strength of the yarns decreases. Benzoxazole hydrolysis causes tensile strength degradation in PBO by disrupting the conjugated rigid rod structure and replacing it with a polyaramid-type structure. Subsequent hydrolysis of the benzamide group causes chain scission and molecular mass decrease, which also contributes to tensile strength degradation [29].

Additional evidence for the breakdown of PBO structure is provided by the SANS analysis. Figure 15 compares SANS images of (a) virgin PBO in D_2O for 5 h, (b) virgin

PBO in D_2O for 36 h, (c) unaged vest yarn in D_2O for 5 h, and (d) vest yarn aged for 157 d in the environmental chamber, in D_2O for 5 h. For unaged and aged vest yarns, the 2D SANS images for 5 h and 36 h were indistinguishable. The corresponding vertical-sector averaged scattered intensity of these three yarns as a function of wavevector, q, are plotted in Figure 16 at 5 h and 36 h.

As shown in Figure 15(a), the 2D SANS image of virgin PBO displays a diamond-shaped scattering pattern, which is indicative of an ordered nanostructure aligned along both the vertical and horizontal directions. After 36 h in D_2O, the relative scattered intensity of the virgin PBO fiber, as shown in Figure 15(b), decreased noticeably, although the diamond shape of the scattering pattern remains the same. This intensity change is believed to reflect the exchange of D_2O and H_2O in the pore spaces of the fiber, which reduces the contrast of scattering between the nanodomain and its surroundings. The lack of changes in the shape of the scattering pattern indicates that no changes in the nanostructure of the fiber have occurred between 5 h and 36 h. The vertical sector averaged scattered intensity for the virgin PBO at 5 h and 36 h, shown in Figure 16, also shows a noticeable difference in intensity near $q \approx 0.3$ nm^{-1}. A broad peak (noted as Point A) is observed in the scattering profile of virgin PBO, and the corresponding length scale of the features that gave rise to this peak is estimated to be approximately 20 nm.

It was expected that the nanostructure of the unaged vest yarn would be similar to that of the virgin PBO; however, the SANS image of the unaged vest yarn (Figure 15(c)) exhibits a vertically preferred pattern only. This result indicates that the ordered-nanodomains were aligned along the horizontal with respect to the incident neutron

direction. No changes in the scattering patterns or scattering profiles were observed between the 5 h and 36 h measurements, in contrast to the behavior of the virgin PBO yarn. It is speculated that D_2O diffusion into the vest yarns occurred completely in the first 5 h, and that no additional diffusion of D_2O occurred between 5 and 36 h. This phenomenaon could be due to differences in internal nanostructure between the virgin PBO spool yarns and the yarns extracted from woven vest fabric, or the fact that there are more damage sites in the vest yarns that provide additional pathways for D_2O ingress. A broad peak at point B in Figure 16, originating from features with length scale approximately 15 nm, is observed in the 15^{o} vertical sector averaged intensity for the unaged vest yarn.

Unlike the SANS images of virgin PBO and unaged vest yarn, the SANS scattering pattern of an aged vest yarn, shown in Figure 15(d), appears to be symmetrical. There is no peak observed in the scattering profiles shown in Figure 16. This scattering profile is similar to that from a random multi-scale structure polymer solution and no ordered nanostructure dominates; i.e. it is postulated that the ordered-nanodomains observed in both the virgin and unaged PBO yarns have broken down after 157 d of environmental exposure. SANS has provided information on PBO nanostructure that is not provided by any other technique. Detailed interpretation of the results, however, will require more controlled experiments to be performed in the near future.

Laser scanning confocal microscope (LSCM) was used to image fibers taken from the vests prior to exposure and after 157 d of exposure, as shown in Figure 17. The vertical banding shown in both micrographs is attributed to mechanical damage incurred

during the weaving process. At the level of observation, no significant changes in surface morphology were observed in the yarns aged for 157 d relative to the unaged yarn.

Atomic force microscopy (AFM) was employed to examine the fiber surface on a smaller scale. Figure 18(a) shows AFM micrographs of the surface of a virgin fiber compared with the surface of a fiber extracted from a woven vest in Figure 18(b). The fiber after weaving, as shown in Figure 18(b), is considerably rougher than the virgin fiber shown in Figure 18(a), further supporting the speculation that mechanical damage is incurred during weaving. This speculation is further reinforced by the comparison of the root mean square roughness (R_q) values of approximately 4 nm for the virgin fiber and approximately 10 nm for the fiber extracted from the woven fabric.

AFM micrographs of fiber surfaces as a function of elevated temperature and humidity exposure are shown in Figure 19. As exposure time increases, this surface roughness also increases. After 9 weeks of exposure (Figure 19(b)) the surface roughness has increased from an R_q of approximately 10 nm to an R_q of approximately 13 nm, however the underlying smooth surface structure is still visible in some areas. After 14 weeks of exposure (Figure 19(c)) the fiber is somewhat smoother, with an R_q value of 6 nm. This lower R_q could be attributed to a sloughing off of some of the larger rough areas of the fiber, thereby exposing the smoother surface underneath. The micrograph taken at 22 weeks (Figure 19(d)) shows a very rough surface, with an R_q value of approximately 20 nm. All traces of the smooth underlying structure seen in Figure 19(a) are completely gone, indicating major degradation of the surface of the fiber.

Tensile testing of the yarns sealed in argon-purged tubes was carried out to determine if the small amount of residual moisture in the fiber was sufficient to initiate

chemical and mechanical degradation. Strength retention data in Figure 20 shows that the sealed tube yarns exhibited less than 4 % loss in tensile strength over the 210 d exposure period, compared to 40 % tensile strength degradation in the same period of time for the yarns exposed to elevated temperature/relative humidity. This result, along with the tensile strength data of yarns extracted from vests placed in a 25 °C and 5 % RH environment, suggest that moisture is an operative factor in chemical hydrolysis, leading to the loss of PBO tensile strength.

The absence of oxygen in the sealed tubes raised the question of whether oxygen alone in or in synergy with moisture could be implicated in PBO degradation. Thermo-oxidative aging studies carried out by researchers at Sandia National Laboratories on nylon 6,6 indicated that the presence of oxygen accelerated hydrolytic degradation mechanisms [30]. It was not feasible to repeat the sealed tube experiments with an oxygen or air atmosphere; however, in isothermal thermogravimetric experiments carried out on PBO yarns in air at 50 °C, mass loss was less than 1 mass % after 18 h. This result suggests that oxidative degradation is not an expected degradation pathway at the temperature employed in the study.

Infrared difference spectra for the yarns aged in the sealed tubes, referenced to virgin PBO, are shown in Figure 21. The largest peak magnitudes are observed for yarns aged for 4 weeks, after which all peaks (positive and negative) grow progressively smaller. The difference spectrum for the 20 week yarn approaches a flat line, indicating that it is almost identical to the virgin PBO reference spectrum. It is postulated that the process of sealing the fibers into the tubes created a reversible perturbation into the system, which gradually dissipated as the aging study commenced. The peak changes

observed in the elevated temperature/humidity study are not in evidence here, and no sign of benzoxazole hydrolysis is observed.

Summary and Conclusions

Tensile strength of yarns extracted from ballistic panels aged at elevated temperature and relative humidity exhibited approximately 40 % loss in strength over a 157 d period. FTIR analysis of yarns exposed to elevated temperature/relative humidity indicated benzoxazole ring opening to yield amide functionality, and subsequent hydrolysis of amide to carboxylic acid and aminophenol groups. Analysis of the fiber surface morphology indicated a surface roughening as a function of exposure time. SANS analysis also revealed differences between the internal structure of virgin PBO spool yarn as compared to PBO vest yarns, in that diffusion of D_2O in the pore spaces of virgin PBO occurred at a slower rate. The scattering profiles of virgin yarn and unaged vest yarn showed internal structure corresponding to size scales between 15 nm and 20 nm, whereas the vest yarns that had undergone 157 d of aging showed no organized nano-structural features in the 20 nm to 200 nm range.

When external moisture was decreased to very low levels, either via storage in a 25 ^{o}C and 5 % RH environment or in argon-purged sealed tubes, changes in yarn tensile strength were less than 4 % and no benzoxazole ring opening was observed via FTIR. These results indicate that one of the main degradation mechanisms in PBO fiber is initiated by moisture, but that moisture inherent in the fiber is not the primary initiator of degradation.

Acknowledgements

The authors gratefully acknowledge project funding provided by the National Institute of Justice (NIJ) as well as the assistance of Ron Rise and Steve Lightsey of the Tekne Group in tensile testing, Nathaniel Waters of NIST's Office of Law Enforcement Standards (OLES) in setting up the temperature/humidity chamber exposures, and Jeff Anderson of the Fabrication Technology Division for preparing the sealed tube samples.

Table 1: Tensile properties of vest yarns during environmental chamber exposure (50 °C/60% RH, 0 days to 84 days, followed by 60 °C/37% RH , 85 days to 152 days); values are averages from all layers tested in two vests. Relative standard uncertainties are typically ± 3 % for tensile strength, ± 3 % for strain, ± 3 % for modulus, and ± 4 % for break energy.

Time in Chamber (d)	Tensile Strength (GPa)	Strain at Break (%)	Modulus (GPa)	Energy to Break Point (N m)
0	4.82	3.31	141.06	0.76
15	4.45	3.09	142.48	0.65
29	4.18	2.96	142.68	0.58
44	4.02	2.88	141.60	0.54
56	3.88	2.73	147.11	0.50
71	3.80	2.71	144.59	0.49
85	3.64	2.55	147.97	0.44
98	3.50	2.50	145.78	0.42
109	3.57	2.51	146.66	0.43
118	3.51	2.48	146.53	0.42
132	3.30	2.40	147.76	0.39
146	3.23	2.28	147.39	0.35
152	3.30	2.31	148.92	0.37
157	3.08	2.17	146.99	0.32

Table 2: FTIR-ATR Band Assignments for PBO Fiber

Band (cm^{-1})	**Assignment**
3097	Aromatic C-H stretch from benzene between oxazole rings, closer to oxygen
3069	Aromatic C-H stretch from benzene between oxazole rings
3040	Aromatic C-H stretch from phenyl ring
2956	Aliphatic C-H stretch (sizing)
2910	Aliphatic C-H stretch (sizing)
2851	Aliphatic C-H stretch (sizing)
1726	
1691	
1619	C=C stretching in substituted aromatic rings, cyclic C=N stretching
1577	Skeletal vibrations in conjugated system/benzoxazole ring
1557	Skeletal vibrations in conjugated system/benzoxazole ring
1496	Skeletal vibrations in conjugated system/benzoxazole ring
1461	Skeletal vibrations in conjugated system/benzoxazole ring
1412	
1367	
1329	C-N stretching
1308	C-N stretching
1276	C-C stretching in carbons linking oxazole and aromatic ring; O-C=N stretching
1210	
1147	Asymmetric stretching of unsaturated cyclic ether
1114	Aromatic C-H in-plane bending
1056	Asymmetric stretching of unsaturated cyclic ether
1010	Aromatic C-H in-plane bending
925	Symmetric C-O-C stretching of cyclic ether
914	Symmetric C-O-C stretching of cyclic ether
869	Aromatic C-H out of plane bending
848	Aromatic C-H out of plane bending
821	Aromatic C-H out of plane bending

Figure 1: Front panels of vests hanging in environmental chamber.

Figure 2: Extraction of PBO yarns from ballistic panels.

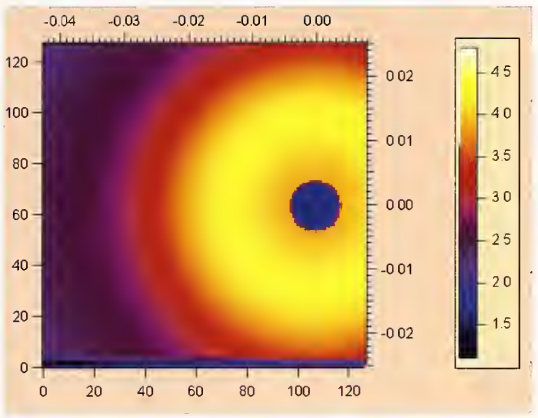

(a)

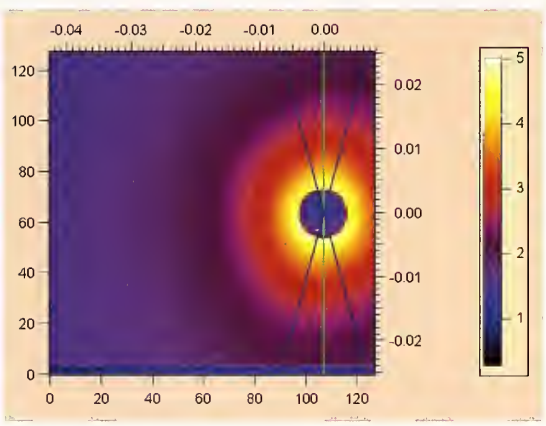

(b)

Figure 3: Two-dimensional SANS images of (a) isotropic, and (b) preferred orientation scattering profiles. In (b) a vertical sector average region of 15 degrees is also illustrated.

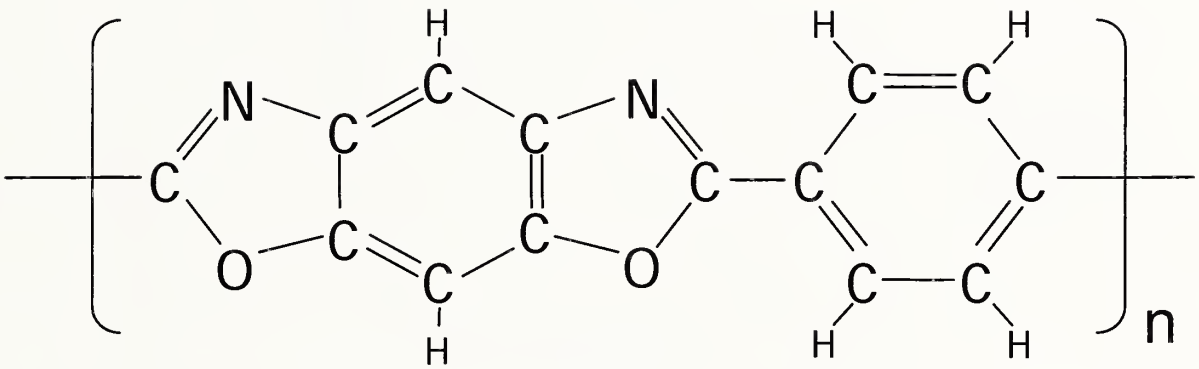

Figure 4: Chemical structure of poly(p-phenylene-2,6-benzobisoxazole), or PBO.

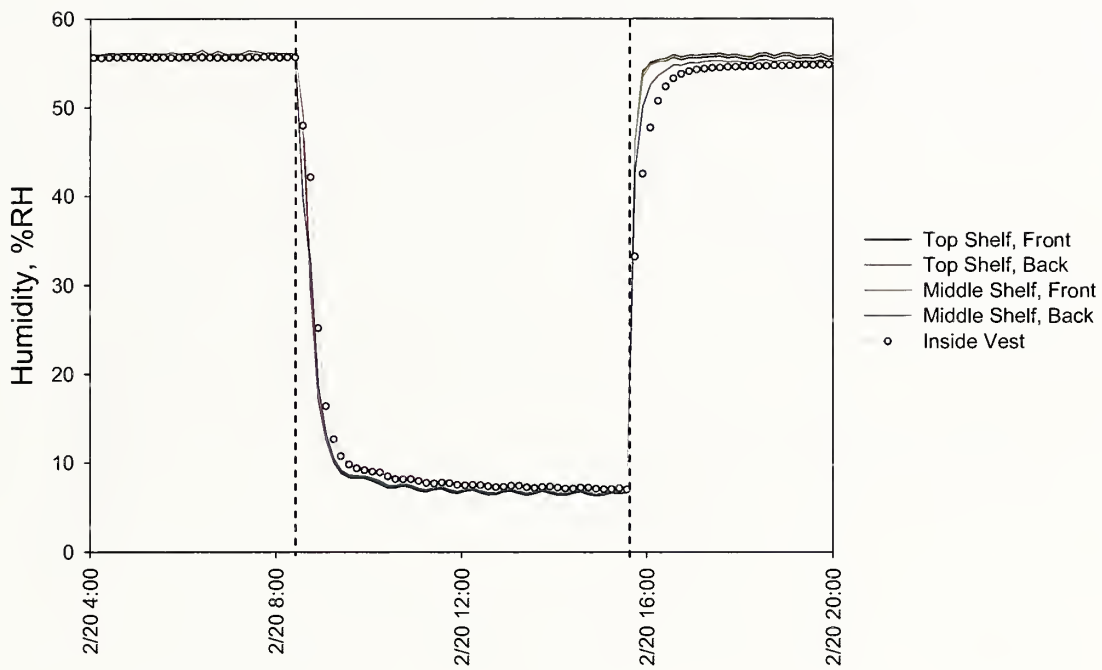

Figure 5: Relative humidity sensor data from environmental chamber, comparing relative humidity at various locations in the chamber to the internal relative humidity of the vest. In the time interval between the dashed lines, the relative humidity settings on the environmental chamber were deliberately decreased and then increased. The estimated uncertainty of the data is ± 2 % RH.

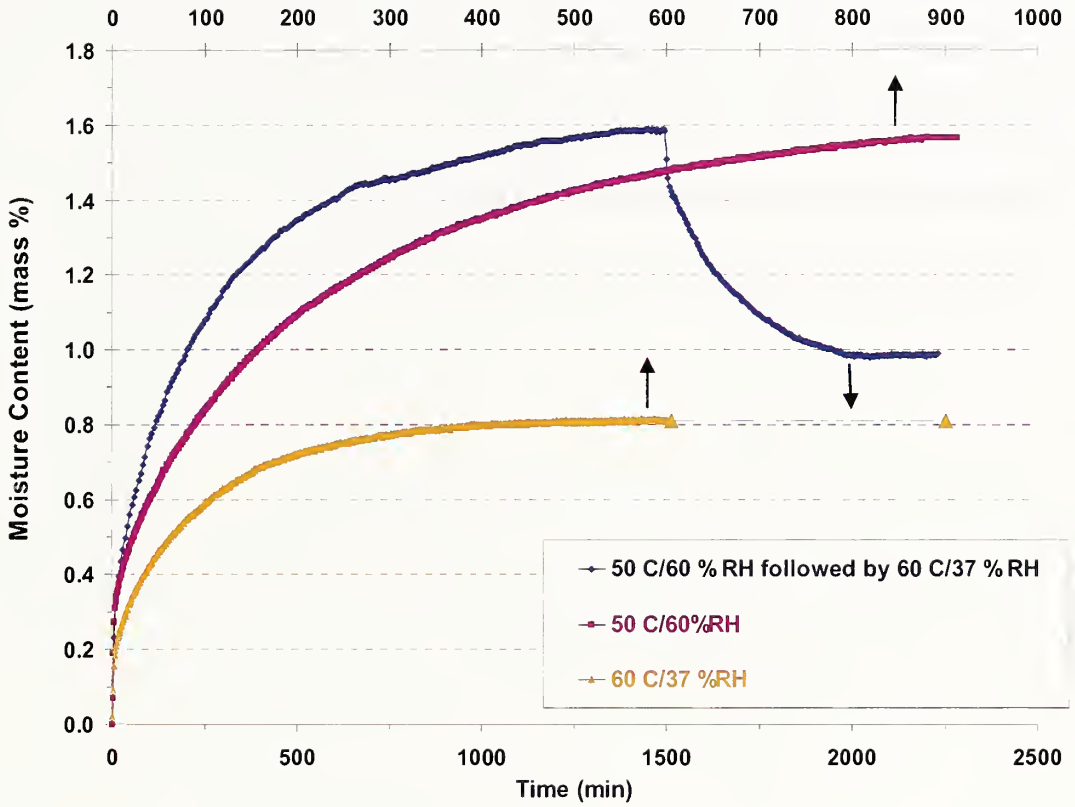

Figure 6: Moisture uptake for virgin PBO yarn measured in separate experiments at (a) 50 °C and 60 % RH, (b) 60 °C and 37 % RH, and (c) 50 °C and 60 % RH and 60 °C and 37 % RH followed by 60 °C and 37 %RH. The estimated uncertainty of the data is ± 0.02 mass %.

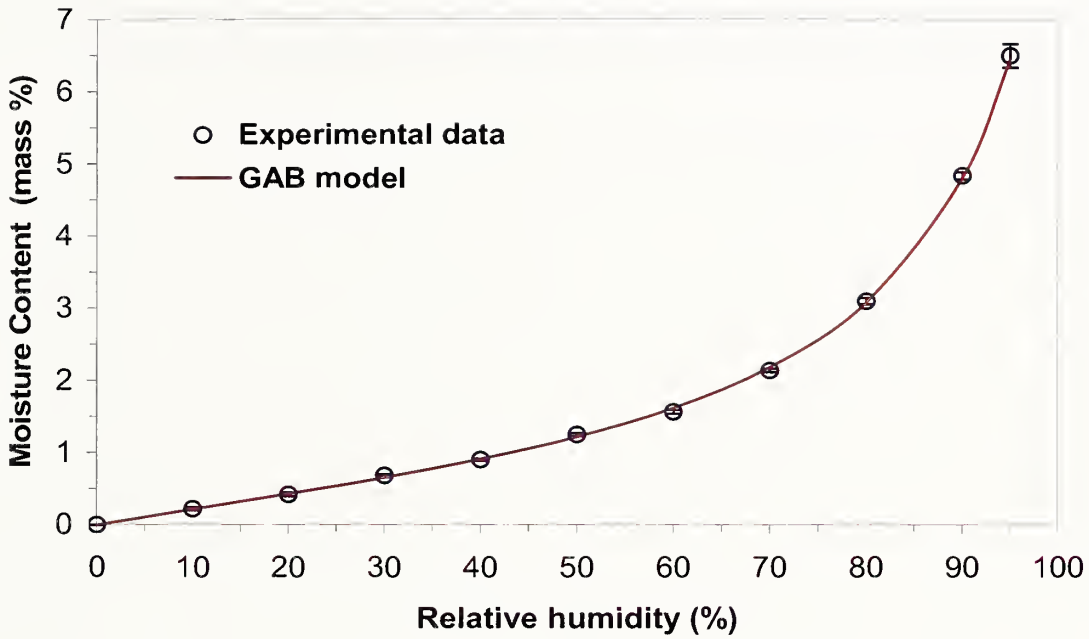

$C_{p,GAB}$	m_{GAB} (%)	k	RSS
2.498	1.00	0.90	0.00977

Figure 7: Water sorption isotherm of virgin PBO yarn at 40 °C. The table provides the parameters obtained from fitting the sorption data to the GAB model.

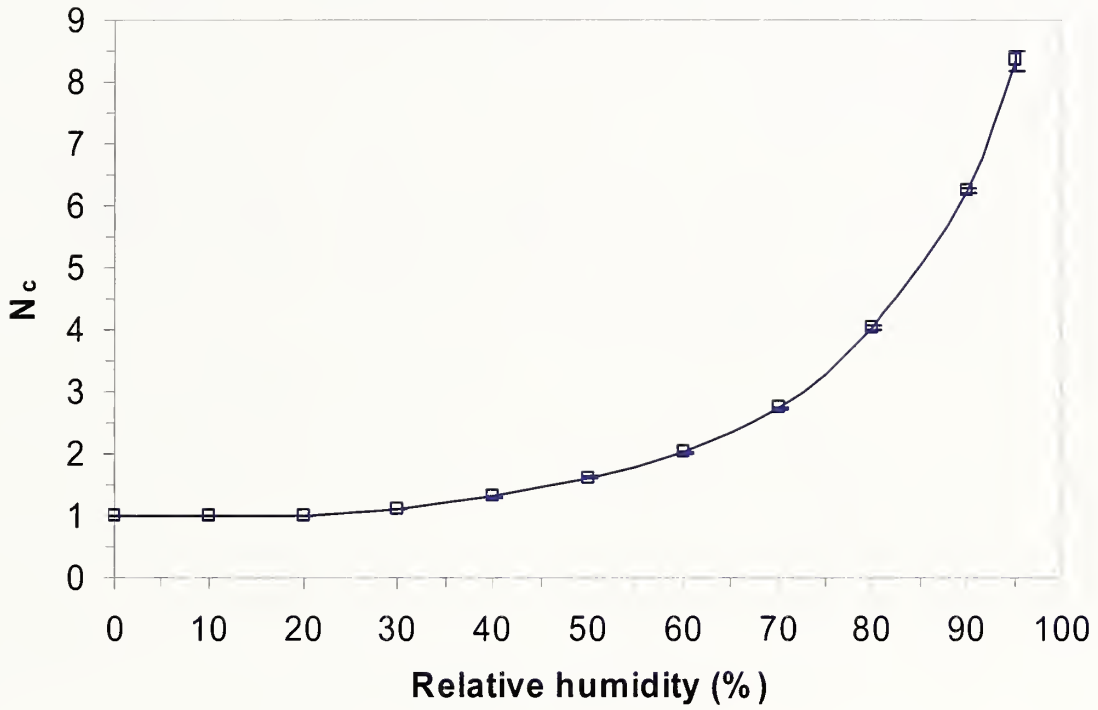

Figure 8: Number of water molecules per cluster, N_c, in virgin PBO yarn, as a function of relative humidity at 40 °C.

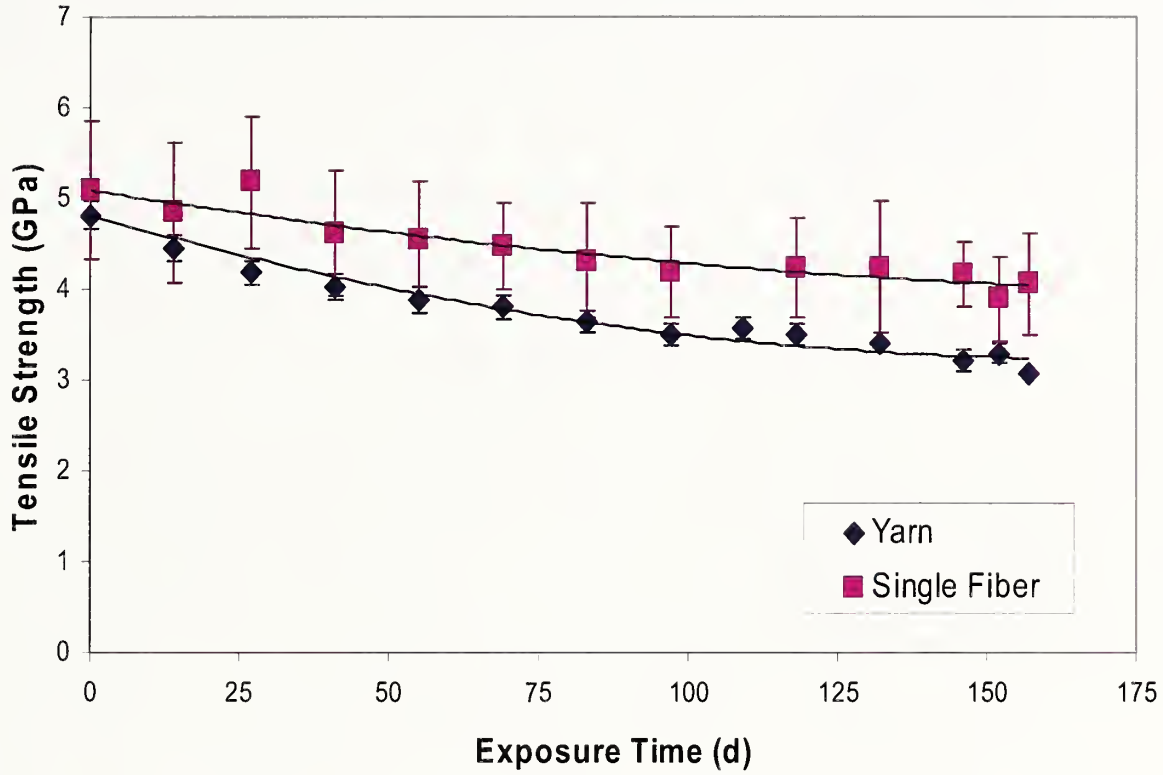

Figure 9: Tensile strength of single PBO fibers measured with DMTA compared to tensile strength of yarns measured on a test frame. Error bars represent one standard uncertainty.

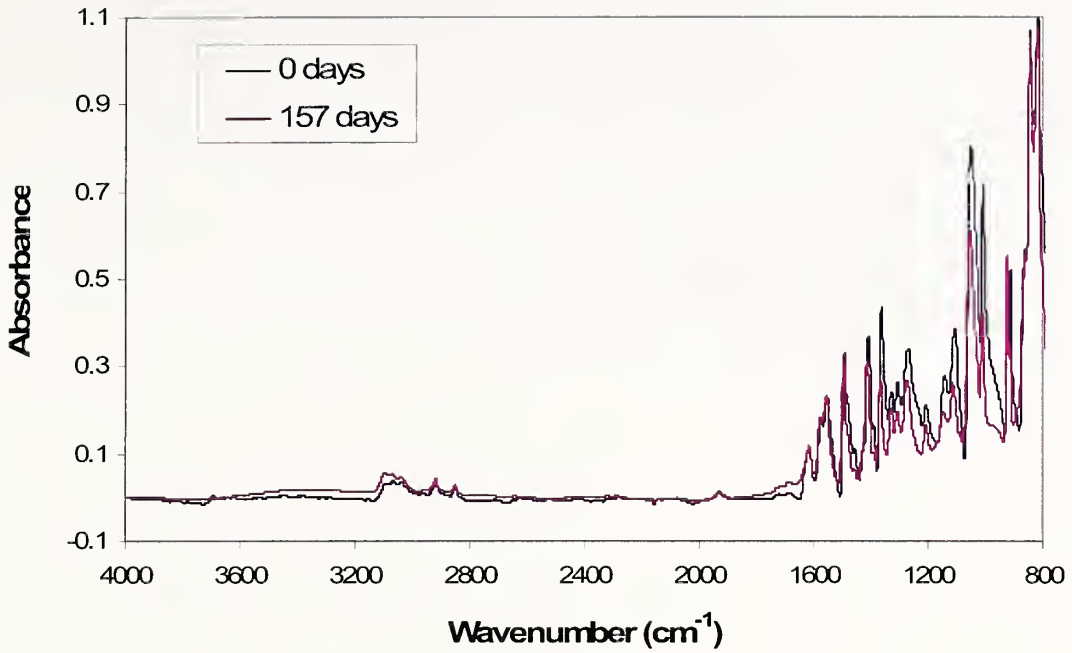

(a)

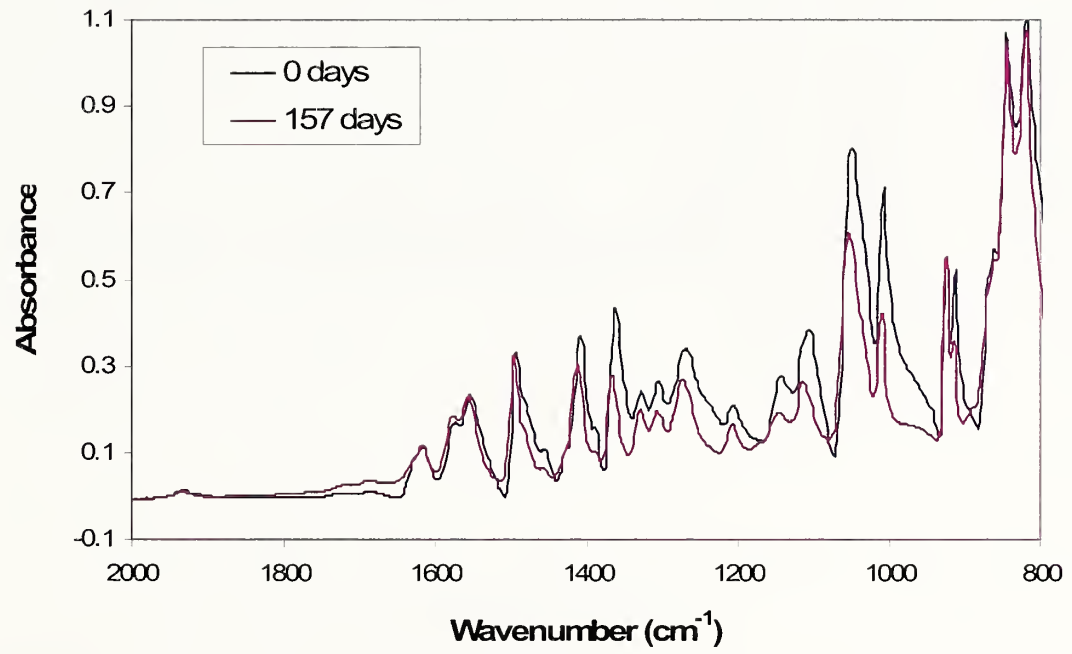

(b)

Figure 10: FTIR spectra of PBO yarns extracted prior to and at the end of temperature and humidity aging. The relative estimated uncertainty of the data is ± 1 %.

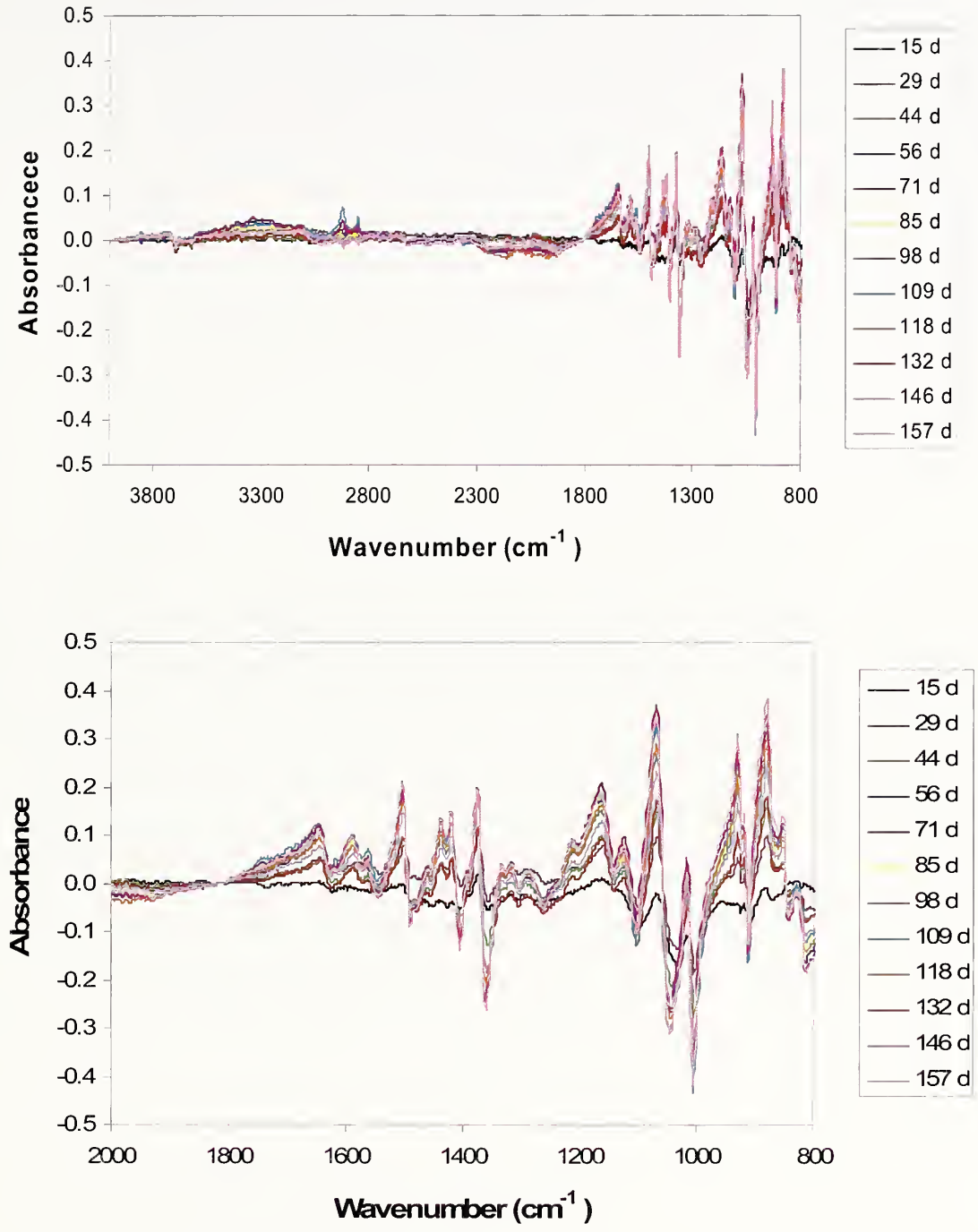

Figure 11: Difference spectra for PBO yarns extracted from aged vests, referenced to spectrum of yarn taken at beginning of exposure.

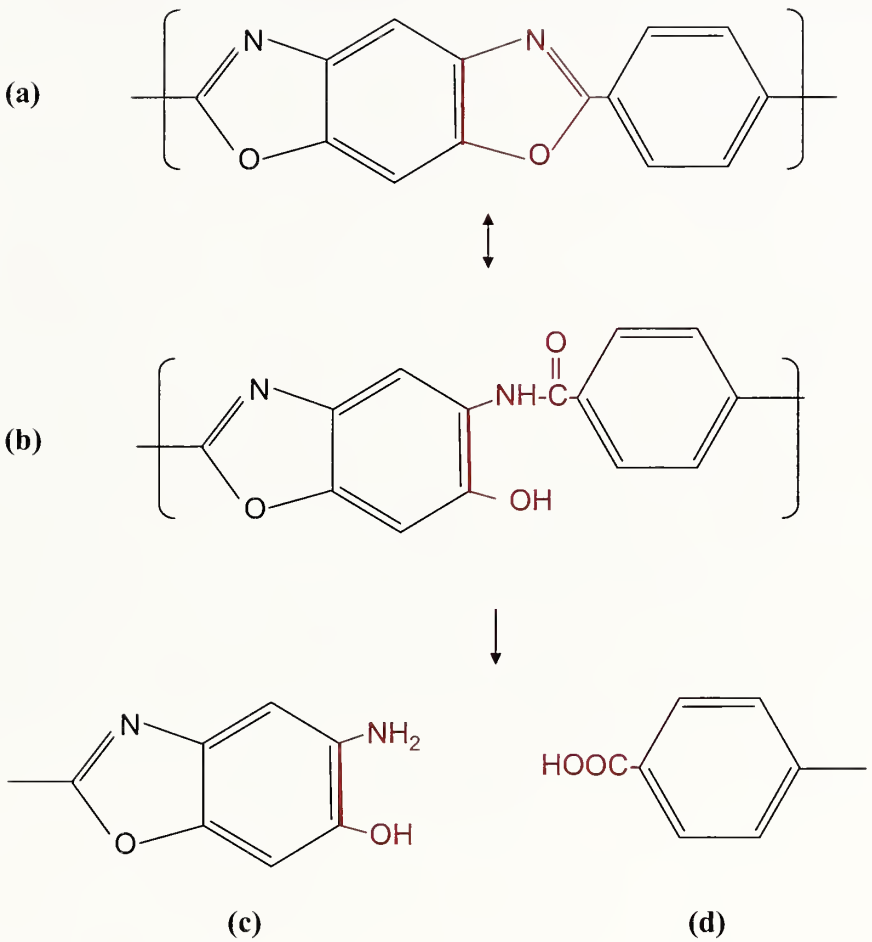

Figure 12: Proposed degradation mechanism, showing benzoxazole (a) conversion to benzamidophenol (b), followed by hydrolysis to aminophenol (c) and benzoic acid (d).

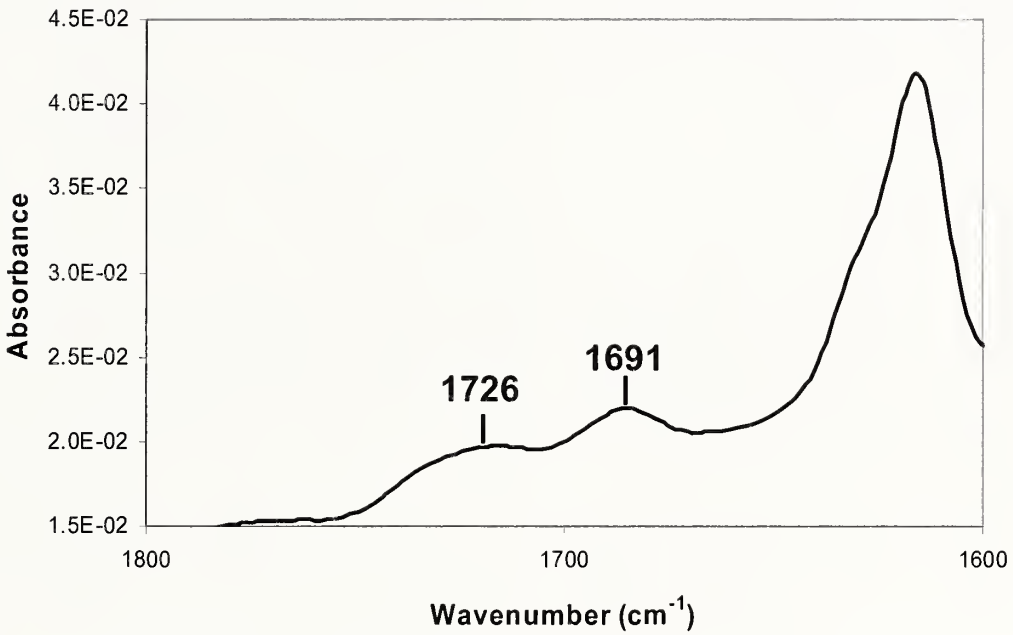

Figure 13: Peaks at 1691 cm^{-1} and 1726 cm^{-1}, observed in the infrared spectrum of all PBO yarns analyzed, tentatively attributed to the presence of phenyl benzoate.

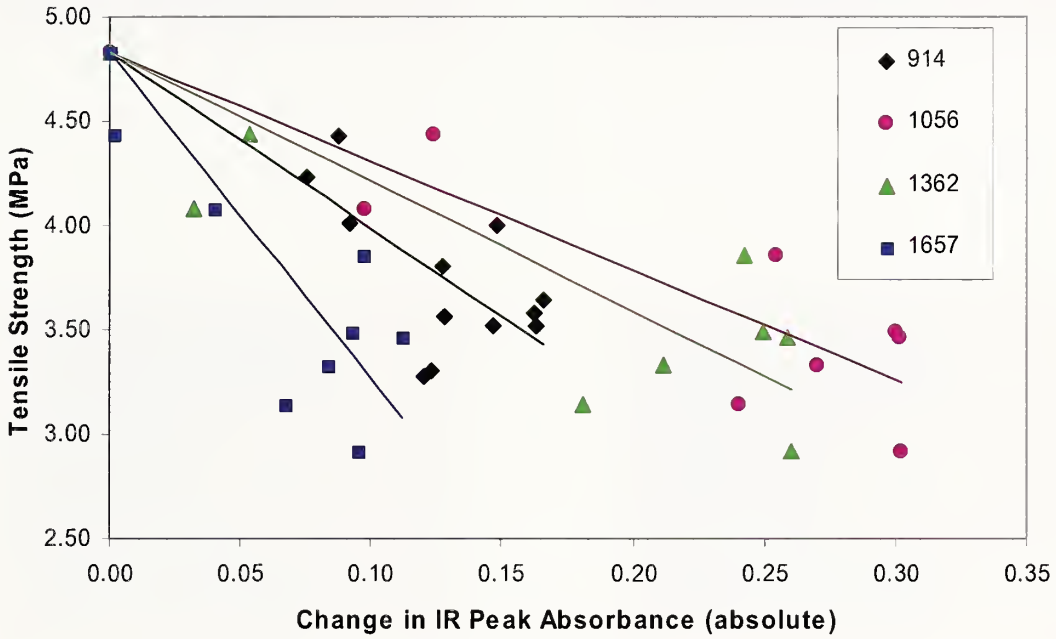

Figure 14: Tensile strength of PBO yarns from aged vests plotted versus the changes observed in infrared peak absorbance.

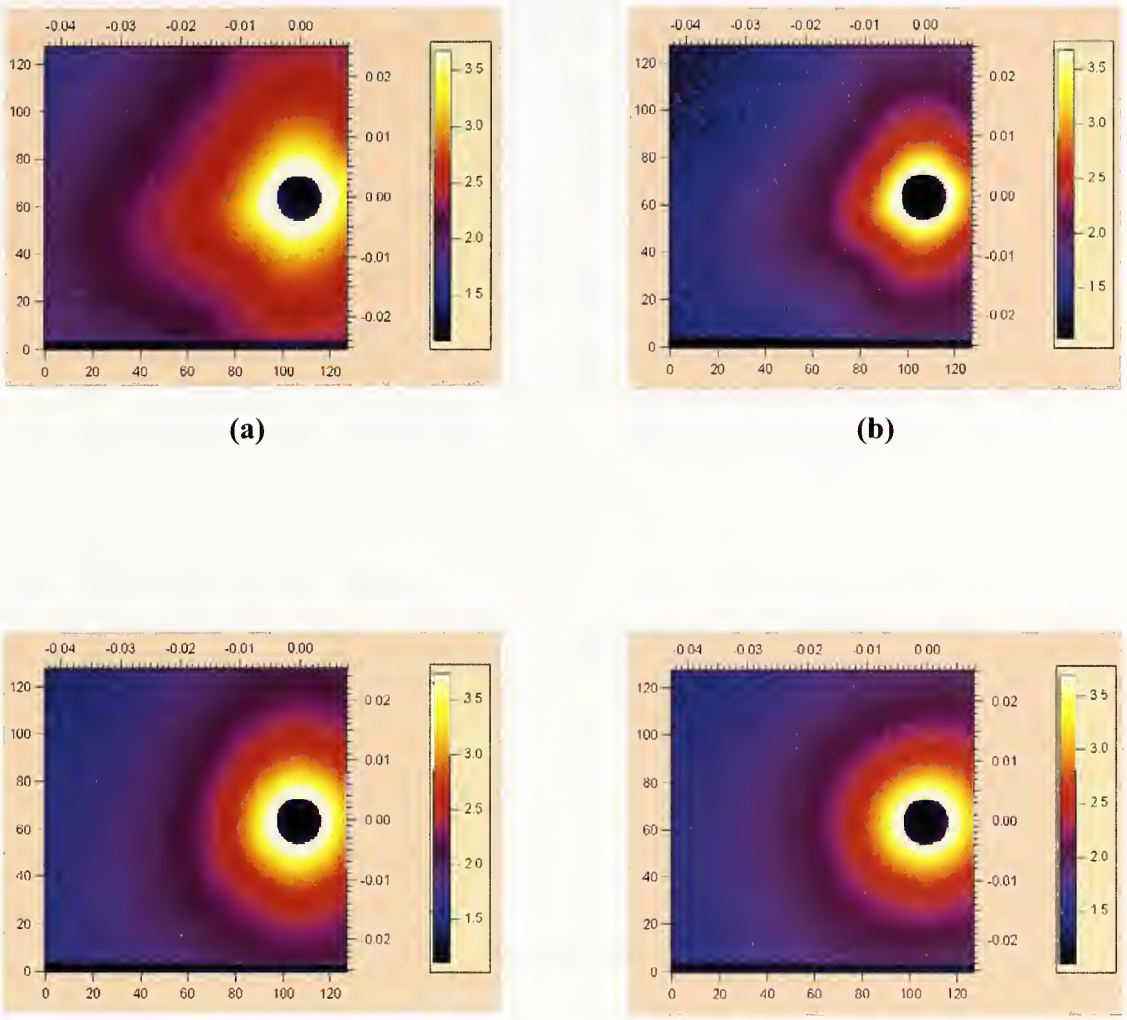

Figure 15: Two-dimensional (2D) SANS images of (a) virgin PBO yarn in D_2O for 5 h, (b) virgin PBO yarn in D_2O for 36 h, (c) unaged vest yarn in D_2O for 5 h, and (d) vest yarn after 157 days of environmental chamber exposure, in D_2O for 5 h. For unaged and aged vest yarns, the 2D SANS images for 5 h and 36 h were indistinguishable.

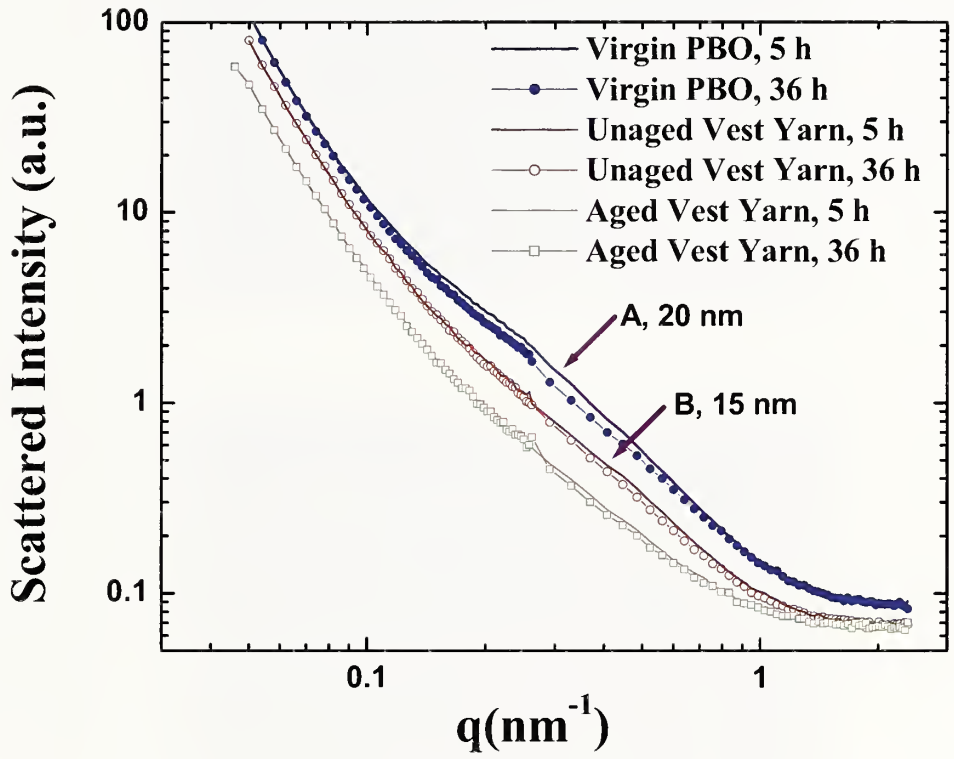

Figure 16: The 15° vertical sector averaged scattered intensity obtained from Figure 15 as a function of wavevector q, for three different yarns in D_2O, measured at 5 h and 36 h. The estimated uncertainty of the data is 1 %.

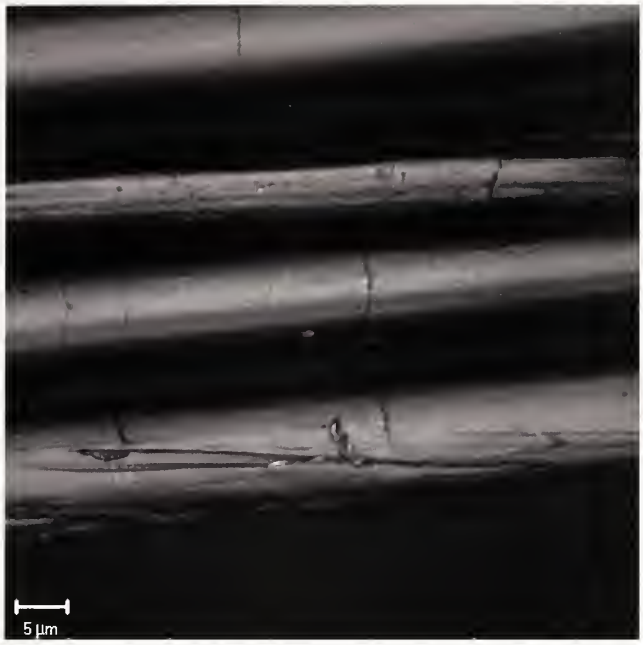

(a)

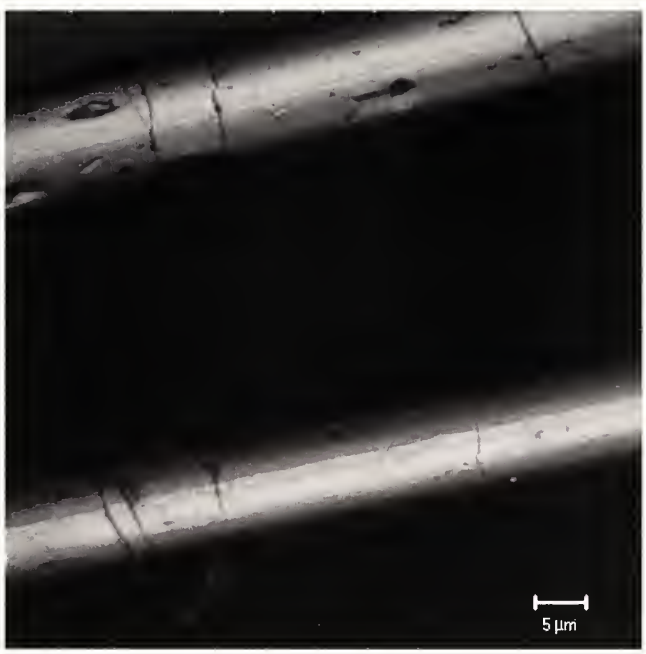

(b)

Figure 17: Confocal images of (a) unaged PBO fiber from ballistic panel, and (b) PBO fiber following 157 d of exposure in environmental chamber.

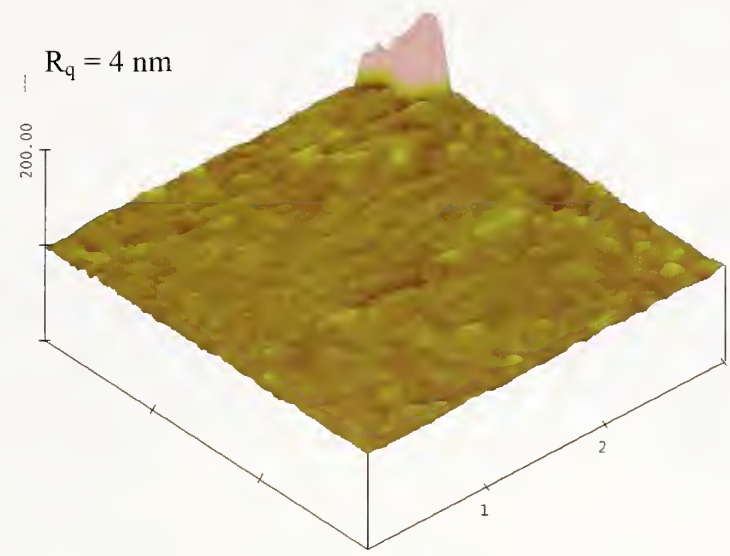

(a)

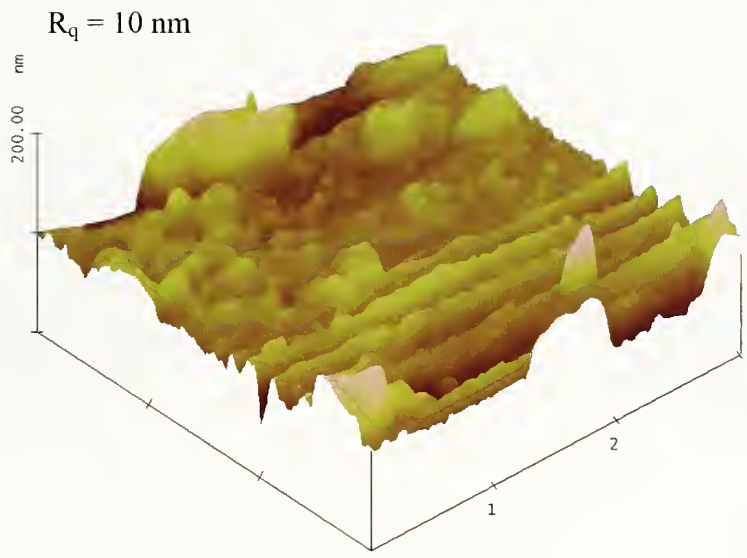

(b)

Figure 18: AFM topographic images and corresponding surface R_q values for (a) surface of virgin PBO yarn, and (b) surface of PBO yarn extracted from unaged woven vest panel. All images are of a 3 μm x 3 μm area and the z scale for all images is 200 nm. The estimated uncertainty of the R_q values is ± 8 %.

R_q = 10 nm

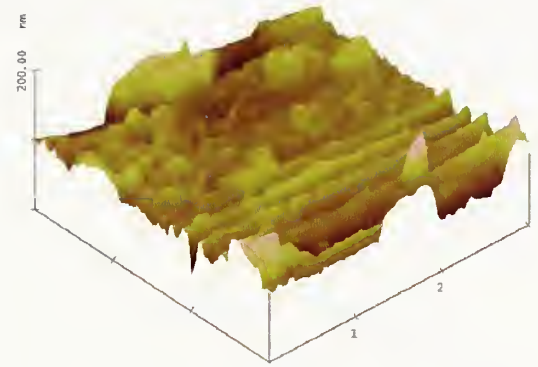

(a)

R_q = 13 nm

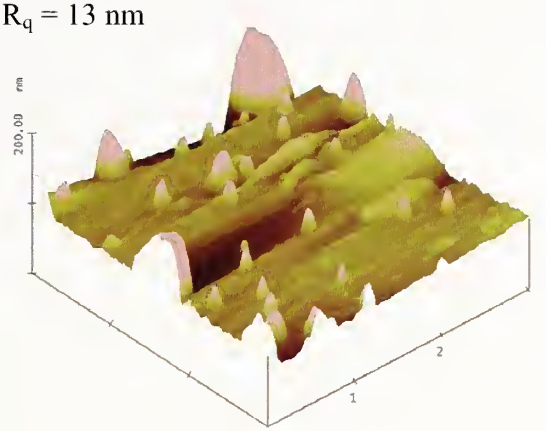

(b)

R_q = 6 nm

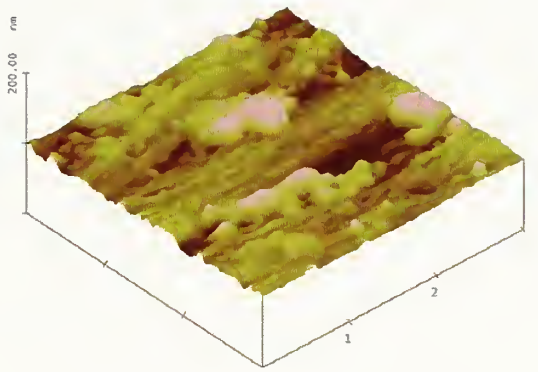

(c)

R_q = 20 nm

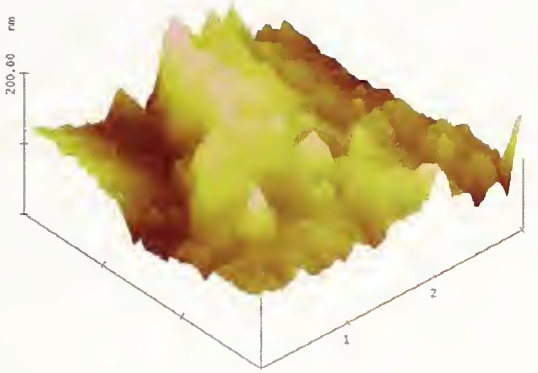

(d)

Figure 19: AFM topographic images and corresponding surface R_q values for fibers extracted from ballistic panels following environmental chamber exposure at (a) 0 d, (b) 56 d, (c) 98 d, and (d) 157 d. All images are of a 3 μm x 3 μm area and the z scale for all images is 200 nm. The estimated uncertainty of the R_q values is ± 8 %.

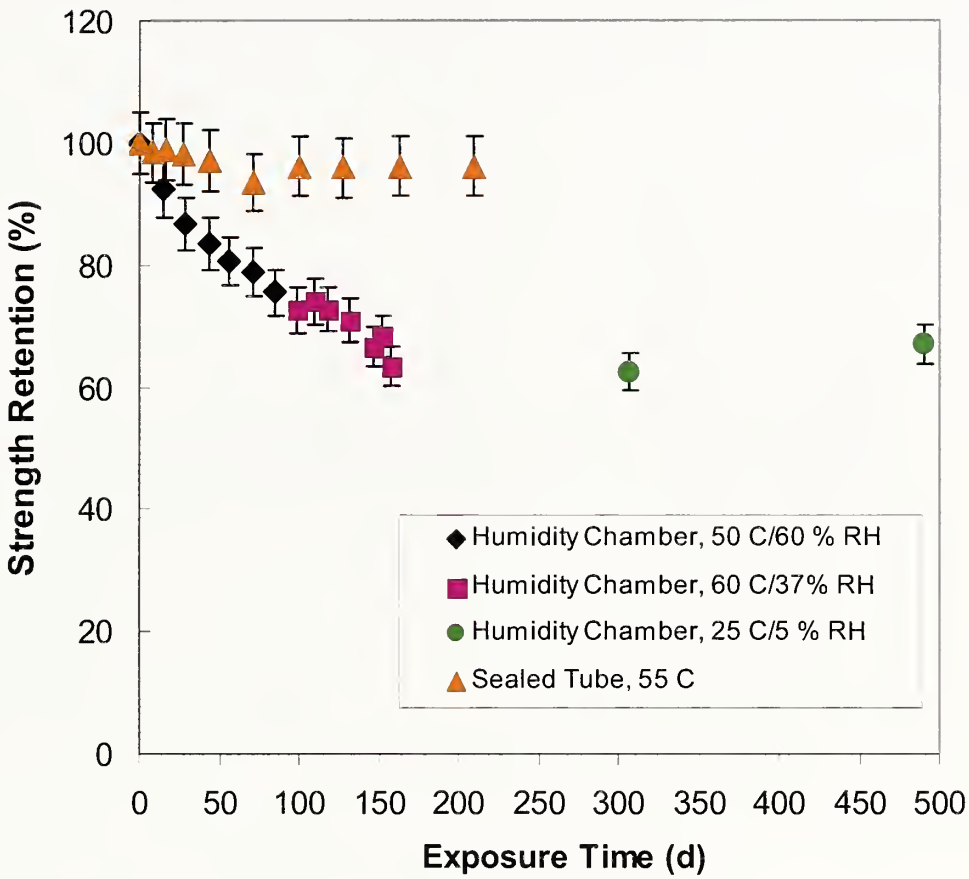

Figure 20: Tensile strength of PBO yarns aged in sealed tubes, compared to tensile strengths of yarns extracted from vests aged in environmental chamber at 50 °C and 60 % RH followed by 60 °C and 37 % RH. Error bars represent one standard uncertainty.

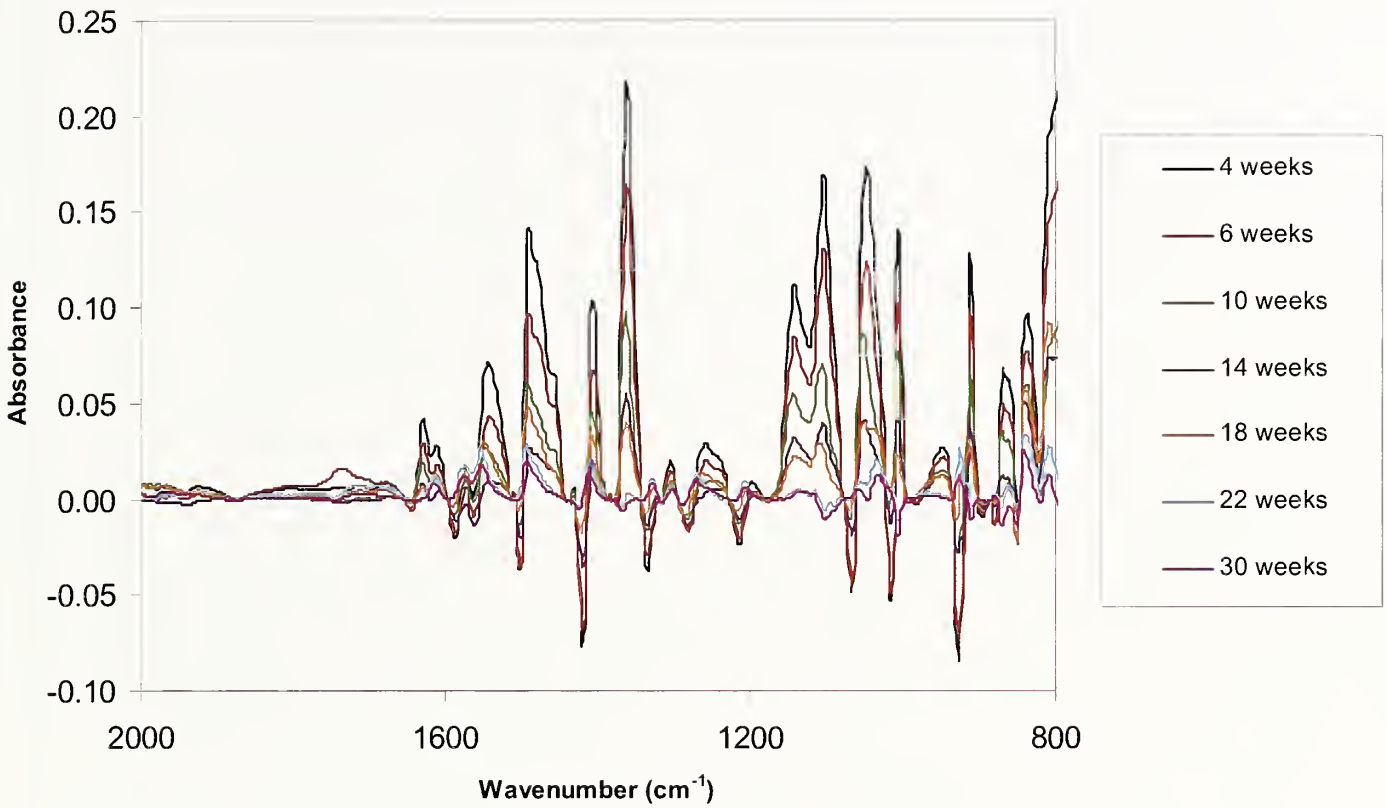

Figure 21: Difference spectra for PBO yarns aged in sealed tubes, referenced to spectrum of virgin yarn.

References

1. Department of Justice Bulletproof Vest Safety Initiative, 03-624 http://www.ojp.gov/pressreleases/DOJ03624.htm.

2. J. Chin, E. Byrd, A. Forster, X.H. Gu, T. Nguyen, K. Rice, W. Rossiter, S. Scierka, J. Sieber, P. Stutzman, and L. Sung, "Chemical and Physical Characterization of Poly(p-phenylene benzobisoxazole) Fibers Used in Body Armor, *NISTIR 7237*, June 2006.

3. ZYLON Technical Information, *http://www.toyobo.co.jp/e/seihin/kc/pbo/menu/fra_menu_en.htm*

4. E. Orndoff, "Development and Evaluation of Polybenzoxazole Fibrous Structures", *NASA Technical Memorandum 104814*, September 1995.

5. B. Dickens in *Service Life Prediction Methodology and Metrologies*, J.W. Martin and D.R. Bauer, eds., (American Chemical Society, 2001).

6. J.S. Higgins and H.C. Benoit, *Polymers and Neutron Scattering* (Clarendon Press: Oxford, UK, 1994).

7. Wolfe, J.F.; *Encyclopedia of Polymer Science and Technology*, *11*, 601.

8. X.-D. Hu, X.-D. S.E. Jenkins, B.G. Min, M.B. Polk and S. Kumar, *Macromol. Mater. Eng.*,**288**, 823(2003).

9. M. Fukuda, M. Ochi, M. Miyagawa, and H. Kawai, *Textile Res. J.,* **61**, 668 (1991).

10. D.A. Mooney and J.M. Don MacElroy, *Chem. Eng. Sci.*, **59**, 2159 (2004).

11. L.-T. Lim, I.J. Britt and M.A. Tung, *J. Appl. Polym. Sci.*, **71**, 197 (1999).

12. M. Fukuda and H. Kawai, *Textile Res. J.*, **63**, (185) 1993.

13. A. Jonquieres and A. Fane, *J. Appl. Polym. Sci.,* **67**, 1415 (1998).

14. Z. Zhang, I. J. Britt, and M. A. Tung, *J. Polym. Sci.: Part B: Polymer Physics*, **37**, 691 (1999).

15. T. Kitagawa, H. Murase, and K. Yabuki, *J. Polym. Sci.: Part B: Polymer Physics*, **36**, 39 (1998).

16. J.F. Fellers and J.S. Lee, Lawrence Livermore National Laboratory Contract P.O. 2819401, *Final Report,* June 1875.

17. M.G. Dobb, D.J. Johnson, A. Majeed, and B.P. Saville, *Polymer,* **20**, 1284 (1979).

18 . M.G. Northholt and J.J. Van Artsen, *J. Polym. Sci. Polym Symp.*, **58,** 283 (1977).

19. K. Tamargo-Martinez, S. Villar-Rodil, J.I. Paredes, A. Martinez-Alonso, and J.M.D. Tascon, *Chem. Mater.*, **15**, 4052 (2003).

20. J.-H. Chang, K. M. Park, S.-M. Lee and J.B. Oh, *J. Polym. Sci. B.*, **38**, 2537 (2000).

21. E.I. Yoo, A.J. Gavrin, R.J. Farris, and E.B. Coughlin, *High Performance Polymers*, **15,** 519 (2003)

22. T. Kubota and R. Nakanishi, *Polymer Letters*, **2**, 655-659 (1964).

23. G. Brana, E. Castellucci and M. Ginanneschi, *Spectrochimica Acta*, **23A**, 751 (1967).

24. R.M. Silverstein, G.C. Bassler, and T.C. Morrill, *Spectrometric Identification of Organic Compounds*, 4th edition (John Wiley and Sons, New York, 1981).

25 . Y.J. Kim, B.R. Einsla, C.N. Tchatchoua, and J.E. McGrath, *High Performance Polymers*, **17**, 377 (2005).

26. Y.-H. So, S.J. Martin, K. Owen, P.B. Smith and C.L. Karas, *J. Polym. Sci: Part A: Polym. Chem.*, **37**, 2637(1999).

27. P.F. Jackson, K.J. Morgan, and A.M. Turner, *J. Chem Soc., Perkin Transactions II*, **2** , 1582 (1972).

28. Y.-H. So, J.P. Heeschen, B. Be.., P. Bon, M. Briggs, R. DeCaire, *Macromolecules*, **31**, 5229 (1998).

29. Y. Termonia, P. Meakin, and P. Smith, *Macromolecules*, **18**(11), 2246 (1985).

30. R. Bernstein, D.K. Derzon, and K.T. Gillen, *Polym. Deg. Stability*, **88**, 480 (2005).